Journal of Materials Research and Technology 35 (2025) 4020–4031

Contents lists available at ScienceDirect

Journal of Materials Research and Technology

journal homepage: www.elsevier.com/locate/jmrt

Advanced post-processing of Ti–6Al–4V alloy fabricated by selective laser melting: A study of laser shock peening and ultrasonic nanocrystal surface modification

A. Amanov [a,*], I.K. Yeo [b], S.H. Jeong [b]

[a] Faculty of Natural Sciences and Engineering, Tampere University, Tampere, 33720, Finland
[b] School of Mechanical and Robotics Engineering, Gwangju Institute of Science and Technology, Gwangju, 61005, Republic of Korea

ARTICLE INFO

Handling editor: L Murr

Keywords:
Ti–6Al–4V alloy
Mechanical properties
Tribology
Additive manufacturing
Peening technology

ABSTRACT

In this study, individual and combined applications of laser shock peening (LSP) and ultrasonic nanocrystal surface modification (UNSM) technologies were applied to Ti–6Al–4V alloy manufactured by the selective laser melting (SLM) process. This study aims to investigate the effects of individual LSP and UNSM technologies, and their sequential combinations in a different order (LSP + UNSM and UNSM + LSP) on the microstructure, grain size, hardness, residual stress, mechanical and tribological properties of Ti–6Al–4V alloy. It is crucial to analyze how the sequential or combined application of LSP and UNSM technologies affects the surface finish of the AM Ti–6Al–4V alloy, which typically has rougher surfaces than traditionally manufactured parts. Results indicated that UNSM technology reduced the surface roughness by about 12 times, introduced a high level of compressive residual stress (CRS), and demonstrated better mechanical and tribological performances than LSP technology. Additionally, the combination of UNSM + LSP technologies, in which LSP technology was subsequently performed on the UNSM-treated sample, was found to be more effective than that of the combination of LSP + UNSM technologies, where the UNSM technology was subsequently performed on the LSP-treated sample.

1. Introduction

Ti–6Al–4V is a Ti-based alloy that gained attention owing to its high specific strength, corrosion resistance, etc., which are essential in aerospace, nuclear and biomedical applications [1,2]. The revolutionary development of the additive manufacturing (AM) process made manufacturing mechanical components made of Ti–6Al–4V alloy possible. Many types of AM technologies are available, and one of them is selective laser melting (SLM), which can print a wide range of materials, including Ti–6Al–4V alloy [3]. However, several critical issues with AM materials must be considered [4]. These issues result from rapid heating and cooling, resulting in high surface roughness, pores and voids, cracking, and tensile residual stress (TRS). The strength and fatigue behavior of AM materials significantly depend on the quality of the surface and inner microstructure [5–10].

Post-processing treatment is an ideal solution to overcome those issues of AM materials. For example, surface milling can smooth a roughened surface of AM materials, while heat treatment can increase the toughness by phase transformation [11–15]. Ma et al. reported the possibility of reducing the surface roughness and increasing the strength of SLM TC4 and TC11 by laser polishing [16]. Moreover, a hot isostatic pressing (HIP) is proposed to reduce the surface and inner microstructure defects of Ti–6Al–4V alloy [17]. However, it may decrease the strength of AM materials. Overall, surface milling and laser peening increase the strength of AM materials, but they cannot fully discard the surface and internal microstructure defects. Applying surface finishing technologies is an ideal method to overcome the microstructure-based issues of AM materials. For instance, shot peening (SP) and laser shock peening (LSP) remarkably enhanced the fatigue strength of Ti–6Al–4V alloy manufactured by powder bed fusion (PBF) thanks to the reduced surface roughness and introduction of compressive residual stress (CRS) [18]. It is also pointed out that LSP technology may extend the service life longer than SP due to the introduced high and deep CRS. Moreover, a high CRS was introduced by laser polishing to extend the fatigue life of AM Ti alloys [19]. Maleki et al. investigated the effect of SP, LSP and ultrasonic nanocrystal surface modification (UNSM) technologies on the fatigue strength of commercially available Inconel 718 superalloy [20]. They concluded that the UNSM treatment induced the highest CRS in the

* Corresponding author.
E-mail address: auezhan.amanov@tuni.fi (A. Amanov).

https://doi.org/10.1016/j.jmrt.2025.02.038
Received 6 December 2024; Received in revised form 4 February 2025; Accepted 5 February 2025
Available online 6 February 2025

surface region, but the LSP treatment introduced the deepest CRS.

UNSM is a mechanical surface treatment technology whose primary source is ultrasonic vibration. This technology has been mainly applied to mechanical parts made of metallic materials. For example, Amanov et al. enhanced the fretting wear resistance of Ti (Gr2) and Ti–6Al–4V alloy (Gr5) by UNSM technology [21]. Nowadays, it is a challenge to have a better surface finish and to achieve a defect-free microstructure of AM materials due to the inevitable surface- and microstructure-related internal defects. Hence, evaluating the effect of UNSM treatment on the surface properties of AM Ti–6Al–4V alloy is of interest. The role of UNSM technology in improving the properties of Ti–6Al–4V alloy is successfully confirmed, where the wear behavior was enhanced by more than 40% due to the reduced surface integrity and porosity, and increased hardness [22]. Moreover, UNSM technology was successfully combined with a local heat treatment, where the sample was heated up during the UNSM treatment [23]. It demonstrated outstanding results, where the hardness of wrought Ti–6Al–4V alloy reached more than 900 HV. After the successful application of high-temperature UNSM technology to wrought Ti–6Al–4V alloy, AM Ti–6Al–4V alloy is also of interest. The surface, mechanical and tribological properties of AM Ti–6Al–4V alloy subjected to high-temperature UNSM technology tremendously improved all the properties of Ti–6Al–4V alloy compared to the as-printed and room-temperature UNSM technology. In addition, it has been pointed out that the UNSM technology resulted in high strength and demonstrated better tribological properties of AM 316L stainless steel [22]. UNSM technology introduces a high CRS within the surface layer and enhances the surface hardness. Still, the adequate effective depth of CRS induced by UNSM treatment is relatively shallower than the LSP technology, which introduces more than 0.8 mm in depth in metallic materials [24–26]. Erfan et al. confirmed the synergy effect of LSP + UNSM technologies on the surface roughness, porosity elimination, mechanical properties and fatigue behavior of AlSi10Mg alloy manufactured by laser-based powder bed fusion (L-PBF) process compared to the single LSP and UNSM treatments [27]. They analyzed the surface roughness and mechanical properties, including hardness, residual stress, strength, and elongation, of AlSi10Mg alloy after applying surface post-processing methods such as LSP, UNSM, and LSP + UNSM. However, the study did not examine the mechanical properties of the UNSM + LSP sequence, even though the order of these treatments can significantly influence material properties. Additionally, it is important to note that in this study, the UNSM treatment was applied parallel to the tensile loading direction of the samples. This study aims to investigate the changes in surface integrity, strength, residual stress, and wear resistance after individual and combined applications of LSP and UNSM technologies to Ti–6Al–4V alloy in a different order and to find the most optimum treatment and order. It is also important to evaluate if the combination of LSP and UNSM technologies is more synergistic and effective than the individual LSP and UNSM treatments.

2. Experimental procedure

2.1. SLM process

SLM (EOS M290, Germany) machine was used to print Ti–6Al–4V alloy samples with an average powder diameter of 50 μm. Tables 1–3 list the parameters of the SLM process, mechanical properties and the chemical composition of the printed samples provided by the supplier, respectively. Additional information about the SLM process can be found in a previous study [22].

Table 1
SLM parameters.

Laser power, W	Scan speed, mm/s	Hatching spacing, mm	Layer thickness, μm
270	110	0.12	50

Table 2
Mechanical properties of Ti–6Al–4V alloy.

Tensile strength, MPa	Yield strength, MPa	Young's modulus, GPa	Elongation, %	Hardness, HV10
1251 ± 61	1120 ± 44	110 ± 7	11.2	310 ± 9

Table 3
Chemical composition of Ti–6Al–4V alloy in wt.%.

Ti	Al	V	C	O	N	Fe	H
Balance	5.5–6.5	3.5–4.5	0.08	0.13	0.03	0.25	0.0125

2.2. LSP and UNSM technologies

The specimens were treated by LSP and UNSM technologies. Schematic views of both the LSP and UNSM treatment processes are depicted in Fig. 1. LSP technology was applied to the samples with an Al coating thickness of 100 μm, as seen in Table 4. Further information about LSP technology is available from a previous study [28]. Individual and combined UNSM treatments were performed on the samples with parameters listed in Table 5. Surface photographs of the untreated (as-printed), LSP-treated, and UNSM-treated samples are shown in Fig. 2. The surface of the untreated sample shown in Fig. 2(a) appears rough, which is typical for Ti–6Al–4V parts produced by the SLM process. Fig. 2(b) presents the surface of the LSP-treated sample, which shows a more organized texture with visible linear patterns. However, it increases the surface roughness of the sample manufactured by the SLM process. It primarily affects the microstructure and mechanical properties rather than drastically altering the roughness of the surface. As shown in Fig. 2(c), the UNSM treatment effectively reduces surface roughness by introducing controlled surface severe plastic deformation (S^2PD) at the nanoscale. The surface of the UNSM-treated sample appears smoother, and more uniform than the untreated and LSP-treated samples. Further detailed information about UNSM technology is available in the previous studies [21–23].

2.3. Tensile test performance

A tensile tester (130–10, KDPI, Korea) was employed to evaluate the tensile properties of the samples under a tensile load of 1000 MPa and a crosshead speed of 5 mm/min in accordance with ASTM E8 standard. Detailed schematic illustrations of the sample geometry with dimensions in mm, build orientation, and LSP and UNSM treatment directions are presented in Fig. 3(a and b), respectively. It is worth mentioning here that LSP and UNSM treatments were applied to both side surfaces without prior polishing. The stress-strain curves of the samples obtained from these tests provide insights into the mechanical response of the Ti–6Al–4V alloy to the applied treatments, capturing variations in yield strength, ultimate tensile strength, and elongation for each treated and untreated sample.

2.4. Dry tribological test

A reciprocating tribometer (Optimol SRV® 5, Germany) was used to assess the effect of LSP and UNSM treatments on the tribological performance of the samples in accordance with ASTM G133 standard at a frequency of 2 Hz, with a stroke of 4 mm for 5000 cycles at a temperature of 25 °C. SAE 52100 bearing steel with a diameter of 7.13 mm reciprocated against the Ti–6Al–4V alloy sample. A coefficient of friction (COF) as a function of reciprocating sliding time was recorded, while the wear resistance was evaluated based on the wear track and total sliding distance.

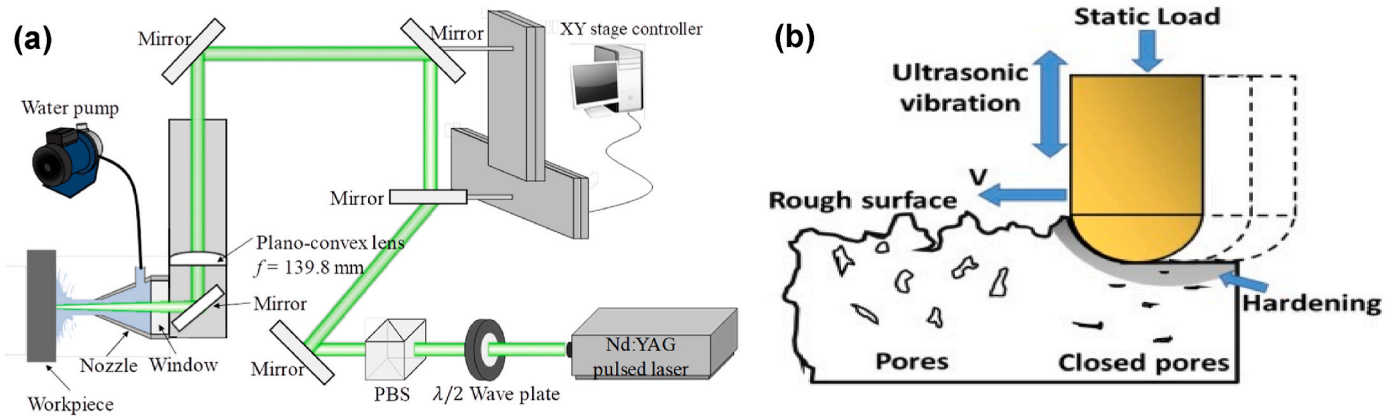

Fig. 1. Schematic view of LSP (a) and UNSM (b) treatment processes.

Table 4
LSP treatment parameters.

Wavelength, nm	Intensity, GW/cm^2	Overlapping ratio, %	Spot diameter, mm	Coating
530	9.5	50	1.18	Al tape

Table 5
UNSM treatment parameters.

Amplitude, μm	Linear speed, mm/min	Static load, N	Interval, μm
30	2000	40	30

2.5. Characterization methods

All the surface characterizations were performed on the as-printed, LSP-treated, UNSM-treated, LSP + UNSM-treated, and UNSM + LSP-treated samples. A surface profilometer (SJ-210, Mitutoyo, Japan) was used to measure the surface roughness. A 3D laser scanning confocal microscope (VK-X210, Keyence, Japan) was used to study the wear track and to calculate the wear rate based on the 2D profile. A hardness tester (MVK-E3, Mitutoyo, Japan) was used to measure the hardness depth profile (HV10). The residual stress values and X-ray diffraction (XRD) patterns were obtained using a Bruker D8 Advance X-ray diffractometer. A scanning electron microscope (SEM: JEOL JSM-6010LA, Japan) and energy dispersive spectroscopy (EDS: JED2300, Japan) were used to investigate the wear degradation mechanisms. A transmission electron microscope (TEM: Titan Themis Z, FEI, USA) was employed to observe the nano-grains.

Fig. 2. Surface photographs of the untreated (a), LSP-treated (b) and UNSM-treated (c) samples.

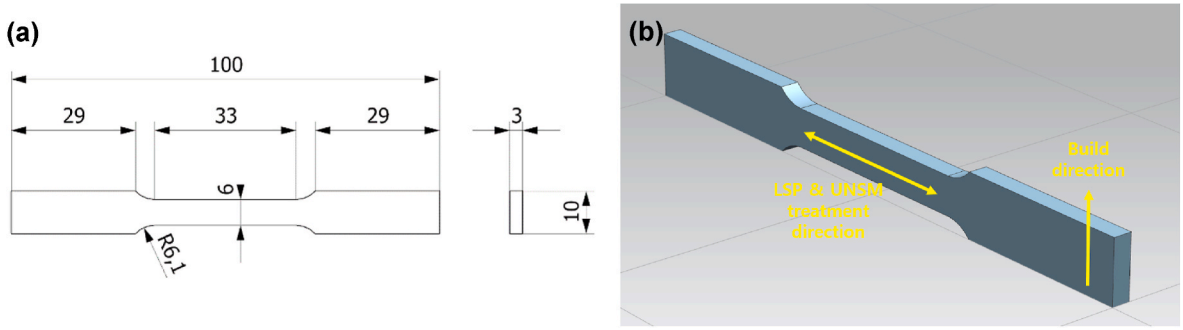

Fig. 3. Schematics of the sample with dimensions (a) and build and treatment directions (b).

3. Results and discussion

3.1. Surface morphology and roughness

SEM images of the untreated, LSP-treated, UNSM-treated, LSP + UNSM and UNSM + LSP technologies are shown in Fig. 4. Fig. 4(a) shows the surface morphology of the untreated sample that appears rough with numerous pits and voids distributed uniformly across the surface. It is generally known that the SLM-manufactured sample surface tends to have a high roughness owing to the presence of porosities, partially melted powder particles, and irregularities [29]. The LSP-treated sample shown in Fig. 4(b) still shows a high density of surface features, but the pits and voids appear slightly less pronounced and are more irregular in shape than the untreated sample. This suggests some degrees of surface modification, but morphology remains relatively rough. It is also clear that partially melted particles were not removed after LSP treatment as shown in Fig. 4(b). The presence of unmelted powders on LSP-treated samples is likely due to the initial SLM process rather than insufficient heat input during LSP. The heat input in LSP is minimal because the process relies on a short-pulsed, high-energy laser that creates a confined plasma explosion, but does not sustain high temperatures long enough to melt or vaporize material. This means that any pre-existing unmelted powders from the SLM process would not be significantly affected or removed by LSP alone. Hence, incomplete melting can leave partially fused or unmelted powders on the surface. As shown in Fig. 4(c), the UNSM-treated sample shows a more uniform and flattened surface than the untreated and LSP-treated samples. The pits and irregularities have been significantly reduced, and the surface appears smoother, likely due to the partially melted particles removed because of the severe plastic deformation of the surface (see Fig. 4(c). SEM images of the samples treated by the combined application of LSP and UNSM technologies in a different order are shown in Fig. 4(d and e). The combination of LSP followed by UNSM treatment (LSP + UNSM) has produced a surface that appears very uniform with minimal pits or irregularities. The morphology is smoother than either LSP or UNSM alone, indicating a synergistic effect when combining both treatments. The other sample, which underwent UNSM first followed by LSP treatment (UNSM + LSP), also shows a smooth, uniform surface like the LSP + UNSM-treated sample. The surface appears slightly less polished than in the LSP + UNSM-treated sample (Fig. 4(d)), with faint surface features visible, possibly due to the sequence of treatments. It was found that the combined application of LSP and UNSM technologies regardless of their order improved the surface morphology of SLM-manufactured samples compared to the individual application.

Fig. 5 shows the average surface roughness (R_a) of the untreated, LSP-treated, UNSM-treated, LSP + UNSM-treated and UNSM + LSP-treated samples. The untreated sample has a higher surface roughness than other samples due to the abundance of pits and irregularities. These features are typically seen on surfaces that have not been modified to improve smoothness or reduce roughness. As mentioned in previous studies, SLM-based samples usually have very rough surfaces [7,30]. The surface roughness of the untreated sample was approximately 9.96 ± 0.90 μm, which was roughened up to 12.10 ± 1.04 μm after LSP treatment. The surface of the LSP-treated sample appeared slightly

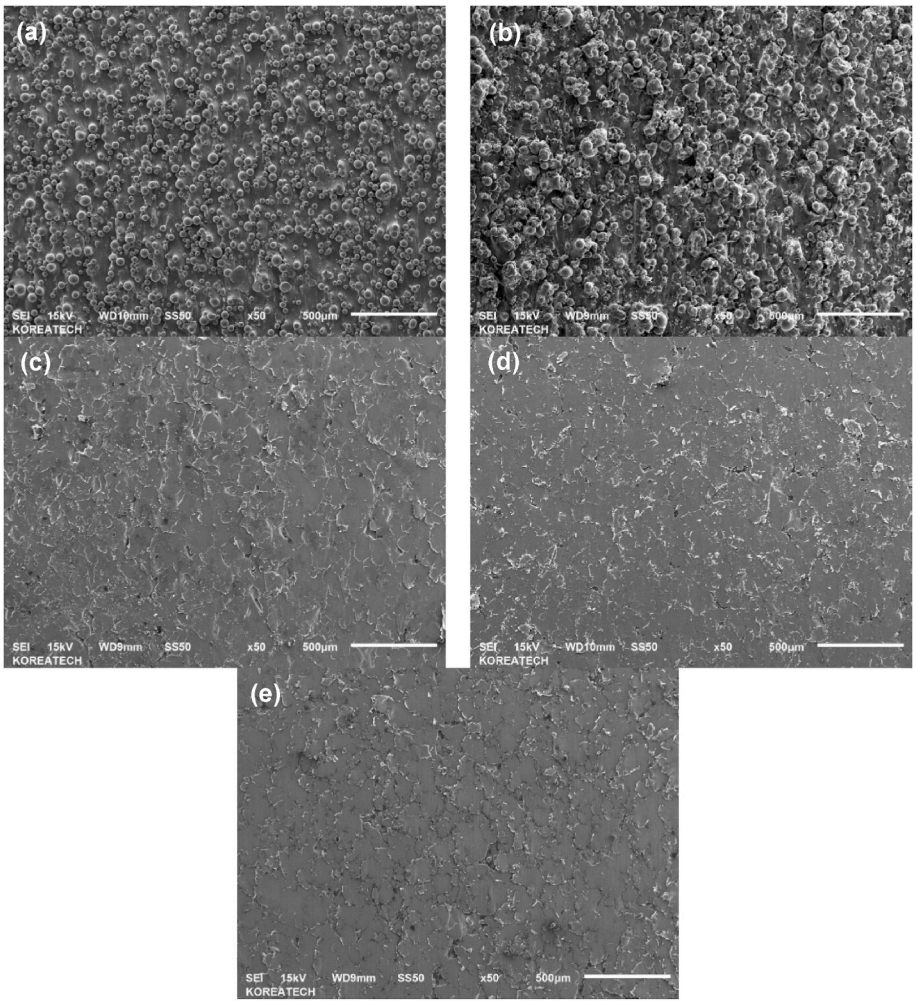

Fig. 4. SEM images of the untreated (a), LSP-treated (b), UNSM-treated (c), LSP + UNSM-treated (d), and UNSM + LSP-treated (e) samples.

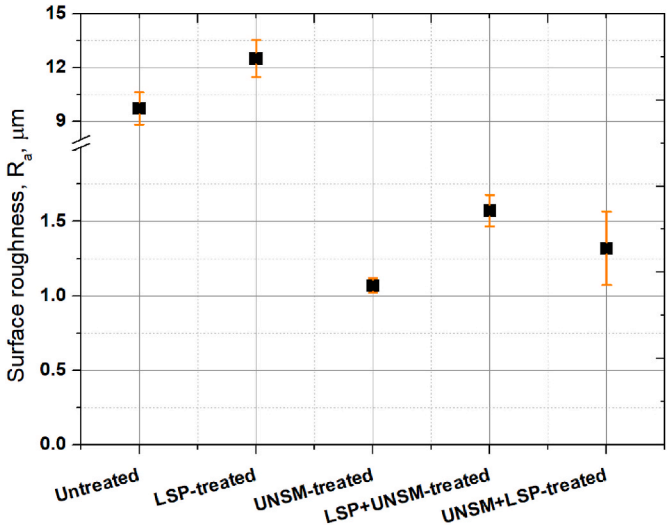

Fig. 5. Surface roughness results of the untreated, LSP-treated, UNSM-treated, LSP + UNSM-treated, and UNSM + LSP-treated samples.

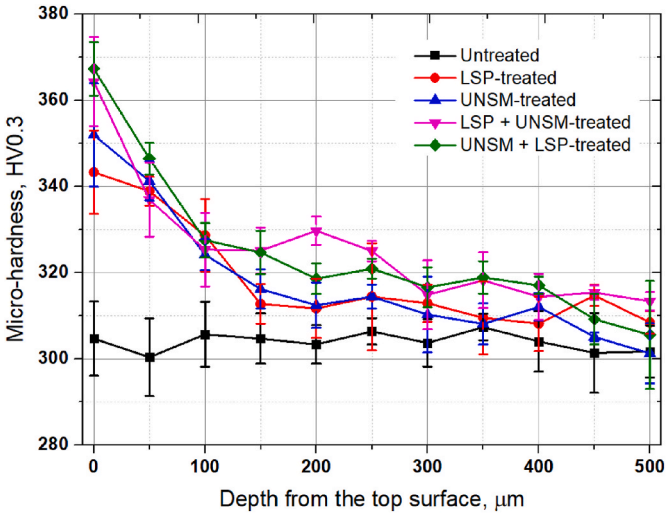

Fig. 6. Vickers hardness depth profile of the untreated, LSP-treated, UNSM-treated, LSP + UNSM-treated, and UNSM + LSP-treated samples.

rougher than the untreated sample due to the presence of numerous small voids. The surface of the untreated samples was tremendously reduced to 1.07 ± 0.06 μm after UNSM treatment, which likely reduced surface asperities, resulting in a finer, more smoothed surface finish. The combination of LSP + UNSM and UNSM + LSP technologies successfully reduced the surface roughness to 1.60 ± 0.11 μm and 1.53 ± 0.25 μm, respectively. However, both the combinations were slightly higher than the individual UNSM treatment because the indents formed by LSP treatment are more significant and profound than the UNSM treatment leading to a rough surface. The effectiveness of UNSM treatment in achieving a smoother and more refined surface compared to the untreated and LSP-treated samples. While LSP treatment primarily enhances subsurface mechanical properties, UNSM treatment directly improves surface finish, making it advantageous for applications where lower roughness and enhanced tribological performance are desired. It has been previously reported that LSP technology leads to high surface roughness when laser energy increases [31] or the overlapping ratio increases [32]. Rough surface roughness may deteriorate wear resistance and fatigue performance and provide crack initiation. For instance, the surface roughness of the material treated by UNSM technology is much better in terms of surface integrity than LSP technology leading to the advancement in tribological and fatigue properties. Hence, the combined application of UNSM and LSP technologies, regardless of their order, has a contributory effect over an individual LSP technology: the smoother surface roughness, the better wear performance, and the longer service life for AM Ti–6Al–4V alloy.

3.2. Vickers hardness

Hardness depth profiles of the untreated, LSP-treated, UNSM-treated, LSP + UNSM-treated and UNSM + LSP-treated samples are shown in Fig. 6. It can be seen that the hardness of the untreated sample was about 304.5 HV. The surface hardness values of the LSP-treated, UNSM-treated, LSP + UNSM-treated and UNSM + LSP-treated samples were 343.3, 352.4, 364.4 and 367.3 HV, respectively. The hardness of the hardened layer was reduced by increasing the depth from the topmost surface, where the effective hardening layer by LSP and UNSM technologies was about ~140 μm. Regardless of their order, the combined application of LSP and UNSM technologies exhibited a deeper hardening effect over individual LSP and UNSM technologies. The UNSM treatment following LSP treatment had the deepest hardened layer with a thickness of about 200 μm. It is well-known that the hardness and dislocation density increase after LSP and UNSM technologies due to the refined grains and S^2PD [33]. Zhang et al. reported that the formation of nano-grains and work-hardening after UNSM treatment dominated and increased the hardness of AM Ti–6Al–4V alloy [34]. It has also been reported earlier that SP enhanced the surface hardness of AM Ti–6Al–4V alloy with similar mechanisms [35,36]. Contrary to the results of the combined application of SP and UNSM technologies [37], the combination of LSP + UNSM and UNSM + LSP technologies in both orders showed a synergy effect on the hardness enhancement. The propagation of shockwaves of LSP treatment might be responsible for further enhancement in hardness in this combination.

3.3. XRD pattern

XRD patterns of the untreated, LSP-treated, UNSM-treated, LSP + UNSM-treated and UNSM + LSP-treated samples are depicted in Fig. 7 (a). The untreated sample shows peaks characteristic of the α-phase (HCP structure) and minor β-phase (BCC structure) peaks. The most prominent peaks are indexed as (100), (101), (102), and (110) for the α-phase and (201) for the β-phase. After LSP treatment, the peak intensities of the α-phase reflections appear to decrease slightly. This indicates that LSP treatment may induce some level of crystallographic refinement, which can reduce peak intensity due to stress-induced modifications. The UNSM-treated sample shows more noticeable changes, with reduced peak intensities and slightly broader peaks compared to the untreated and LSP-treated samples. This broadening can suggest increased dislocation density and grain refinement due to the severe plastic deformation from UNSM treatment. Additional high-intensity peaks such as (002) and (202) suggest that combining treatments may alter the phase composition or induce preferred orientation in certain crystallographic planes. It can also be noticed from Fig. 7(b) that the peaks of the (002) and (101) shifted to lower diffraction angles, which were caused by micro-strain, grain size refinement, and other microstructural-related factors. This shift also suggests the introduction of CRS within the surface layers, as it generally causes a contraction in lattice spacing. The combination of LSP and UNSM treatments shows the largest shifts in peak positions. This indicates a cumulative effect of both treatments, generating significant CRS and possibly higher strain in the surface region, which improves the mechanical performance of Ti–6Al–4V alloy, especially in applications requiring high fatigue and wear resistance. The sequential treatments (LSP + UNSM and UNSM + LSP) yield the most substantial increases in peak intensity and broadening, implying enhanced grain refinement and possible crystallographic reorientation. This suggests that combining LSP and UNSM

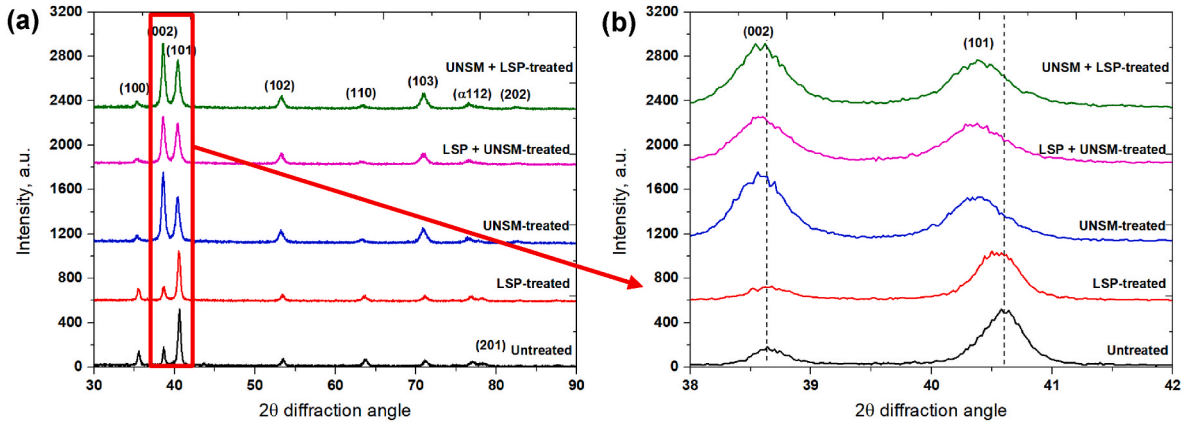

Fig. 7. XRD patterns (a) and shift (b) of the untreated, LSP-treated, UNSM-treated, LSP + UNSM-treated, and UNSM + LSP-treated samples.

creates a synergistic effect on the microstructure of Ti–6Al–4V alloy. Hence, the LSP and UNSM technologies could refine coarse grains and induce CRS [38,39]. Moreover, the higher surface roughness of LSP technology than other peening technologies may result in a high level of lattice distortion. A widening of full width at half maximum (FWHM) of α phase (101) took place, leading to an increase in dislocation density after LSP and UNSM technologies [40]. FWHM of (002) and (101) peaks can be seen in Table 6 below, where the grain growth of the beta phase for the UNSM technology and its combination with LSP technology occurred. In addition, the diffraction peaks of the samples shifted toward lower angles (see Fig. 7(b)). Based on Bragg's law, the shift in diffraction angle means a change in the lattice plane related to the prevailing martensitic transformation [41] (see Table 7).

3.4. Surface residual stress

Fig. 8 shows the measured surface residual stress of the untreated, LSP-treated, UNSM-treated, LSP + UNSM-treated and UNSM + LSP-treated samples. It is commonly known that the untreated sample has a TRS near the surface, which was attributed to the rapid cooling during the SLM process [8,42]. As expected, TRS was converted into high CRS after LSP, UNSM, LSP + UNSM and UNSM + LSP technologies (see Fig. 8). The combined application of LSP + UNSM technologies introduced the highest CRS value of −705 MPa, which is higher than individual LSP and UNSM technologies attributing to the repeated impact to the surface. However, the CRS of the UNSM + LSP-treated sample was weaker than the UNSM-treated sample. In subsequently, LSP technology released the CRS introduced by UNSM technology. It is similar to the earlier reported phenomena of the combination of UNSM and SP technologies [37], where the UNSM technology after SP treatment resulted in the release of CRS due to relaxation. This significant enhancement of CRS can enhance the wear and fatigue performance of the AM materials. LSP technology tends to induce deep CRS, which improves fatigue performance, and delays crack propagation [43,44]. At the same time, UNSM treatment also increases fatigue strength owing to the introduced CRS and nano-grains of AM material [45]. It is well-known that LSP treatment induces very deep CRS at the subsurface, but less CRS at the top surface, while UNSM treatment induces very high CRS at the top surface, but less CRS at the subsurface. Hence, it is meaningful to combine these two LSP and UNSM technologies to induce simultaneous intense and high CRS at the top and within the surface layers. The SP process also showed the introduction of CRS to the AM Ti–6Al–4V alloy, which increased fatigue strength [35].

Table 6
Micro-strain and FWHM values of 101 peaks.

Samples	Micros-strain (101)	FWHM (101)
Untreated	–	0.41128 ± 0.00482
LSP-treated	0.00947 ± 0.00062	0.42312 ± 0.00452
UNSM-treated	0.05784 ± 0.00185	0.55269 ± 0.00847
LSP + UNSM-treated	0.05548 ± 0.00178	0.54451 ± 0.00966
UNSM + LSP-treated	0.05898 ± 0.00157	0.56198 ± 0.00852

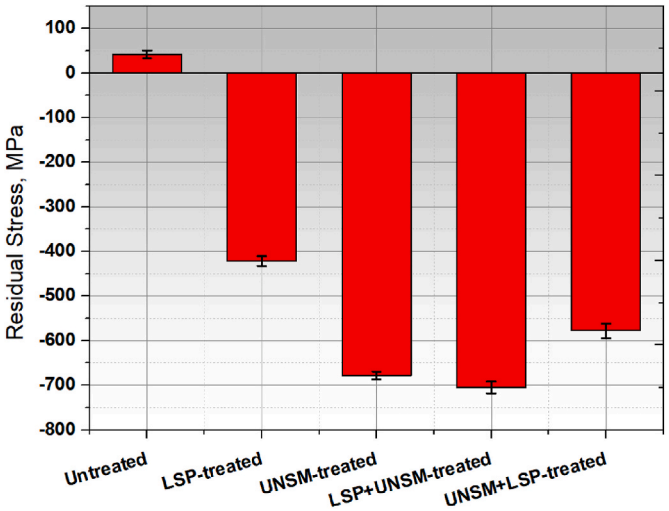

Fig. 8. Surface residual stress of the untreated, LSP-treated, UNSM-treated, LSP + UNSM-treated, and UNSM + LSP-treated samples.

3.5. Mechanical properties by tensile test

Plotted stress-strain data of the untreated, LSP-treated, UNSM-treated, LSP + UNSM-treated and UNSM + LSP-treated samples are depicted in Fig. 9(a). The untreated sample demonstrated the lowest tensile strength and elongation. Typically, AM Ti–6Al–4V alloy has poor ductility due to a fine and fully α-martensite phase [2]. It has been discovered that LSP and UNSM technologies could improve the tensile properties. The tensile strength results showed similar correlations to the hardness test results, as summarized in Table 7. The UNSM + LSP-treated sample had the highest tensile strength and elongation (1250.893 MPa and 12.80%) among the LSP-treated, UNSM-treated, and LSP + UNSM-treated samples, respectively (see Fig. 9(b)). Moreover, linear elastic deformation and yield plateau stages were also observed as shown in Fig. 9(c), wherein in the elastic deformation stage, the microstructure of the samples underwent micro-scale bending. Subsequently, the second stage was initiated due to critical stress, where the microstructure was further deformed. However, the LSP and UNSM technologies have no beneficial effect on strength and strain due to the

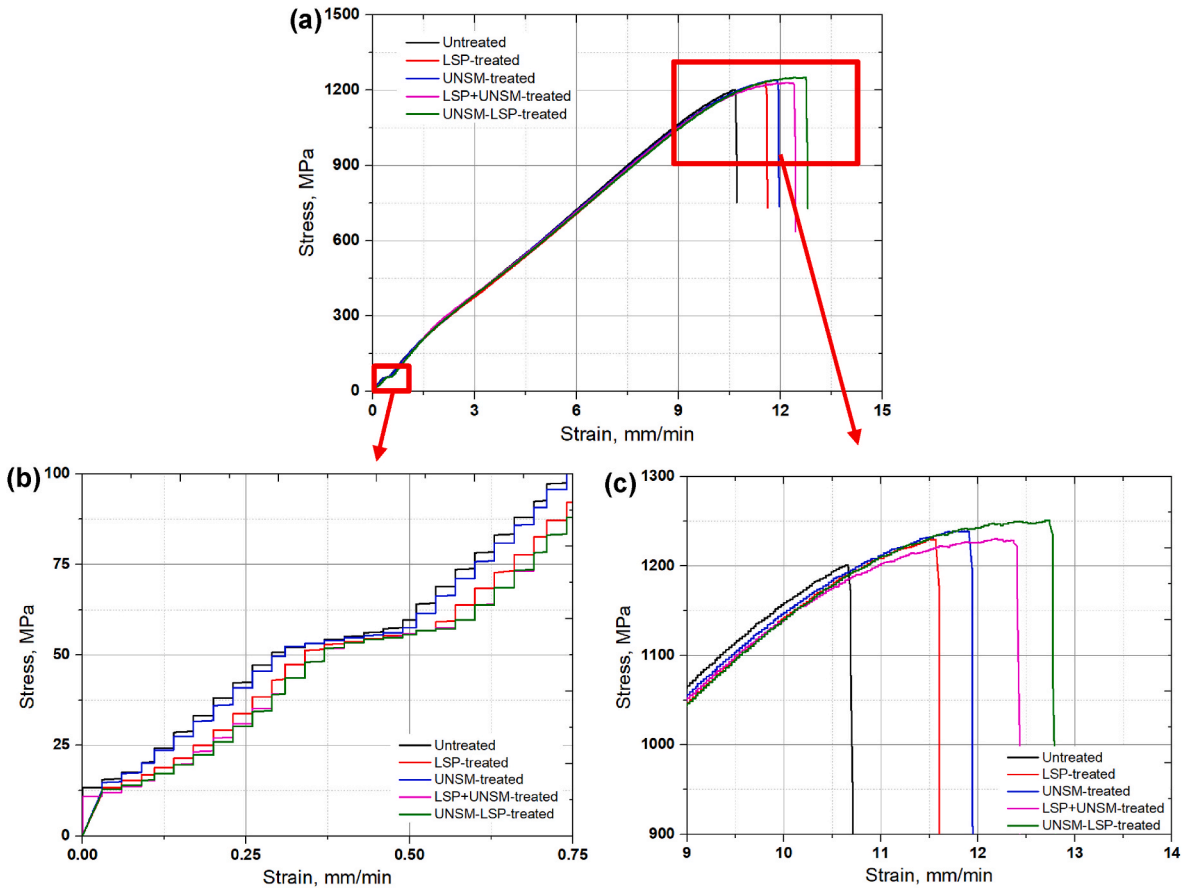

Fig. 9. Stress-strain curves of the untreated, LSP-treated, UNSM-treated, LSP + UNSM-treated and UNSM + LSP-treated samples.

Table 7
Mechanical properties of the samples derived from tensile tests.

Samples	Load, kgf	Tensile strength, MPa	Gauge length, mm	Max displacement, mm	Elongation, %
Untreated	2204.5	1201.042	35	3.75	10.71
LSP-treated	2257.5	1229.917		4.07	11.63
UNSM-treated	2275.0	1239.452		4.19	11.97
LSP + UNSM-treated	2258.0	1230.190		4.35	12.43
UNSM + LSP-treated	2296.0	1250.893		4.56	12.80

elastic region in these stages. Lu et al. tailored a gradient nanostructure that improves strength and ductility simultaneously [46]. Hence, it is proposed that the formation of a gradient nanostructure by LSP and UNSM technologies tends to enhance tensile strength and elongation. The UNSM-treated sample had a similar tensile strength to the LSP + UNSM-treated sample, but the elongation was poorer than the LSP + UNSM-treated sample.

3.6. Top surface TEM

The TEM images in Fig. 10 provided the nanostructural differences on the top surface of SLM Ti–6Al–4V alloy samples subjected to LSP, UNSM, LSP + UNSM and UNSM + LSP treatments. These images also highlight the distribution and morphology of the α and β phases, which are key microstructural constituents in Ti–6Al–4V alloy. It was observed that all the treatments resulted in a transformation from coarse grains to nano-grains. As shown in Fig. 10(a), the LSP-treated sample shows well-defined α lamellar structures with dispersed β phase regions. The α phase appears as elongated lamellae, while the β phase is found in darker, more isolated regions. The UNSM-treated sample shows a more refined microstructure with a reduced α lamellar width and more uniformly distributed β phases, which appear somewhat elongated and dispersed across the matrix (see Fig. 10(b)). The LSP + UNSM-treated sample demonstrates a complex microstructure with both refined α lamellae and dispersed β phases (see Fig. 10(c)). The α lamellae are thinner than in the individual treated samples, while the β phase is distributed more uniformly. As shown in Fig. 10(d), the UNSM + LSP-treated sample shows a similar, but slightly more refined nanostructure than the LSP + UNSM-treated sample. The α lamellae are finely distributed, and the β phase is dispersed to indicate a higher degree of grain refinement. Moreover, individual LSP, the combination of UNSM + LSP and LSP + UNSM technologies were able to form a lamellar structure (see Fig. 11(b, c, and d)), which was smaller than that of the range reported in the literature [47]. According to the Hall–Petch equation the LSP-treated sample exhibited a bit lower surface hardness than the UNSM-treated sample, which may be associated with the higher grain size [48]. LSP, UNSM and their combinations induce CRS and increase dislocation density within the surface layers. This CRS refines the α-β interface, making the lamellar α phase more prominent. The increased stress and strain by these technologies can also enhance phase boundary strengthening. Moreover, the refined microstructure suggests that both LSP and UNSM technologies enhance surface strength and wear resistance due to the high density of grain boundaries, which act as obstacles to dislocation motion. The alternating layers of LSP and UNSM likely increase the strain hardening within the material, refining the α and β phases. When

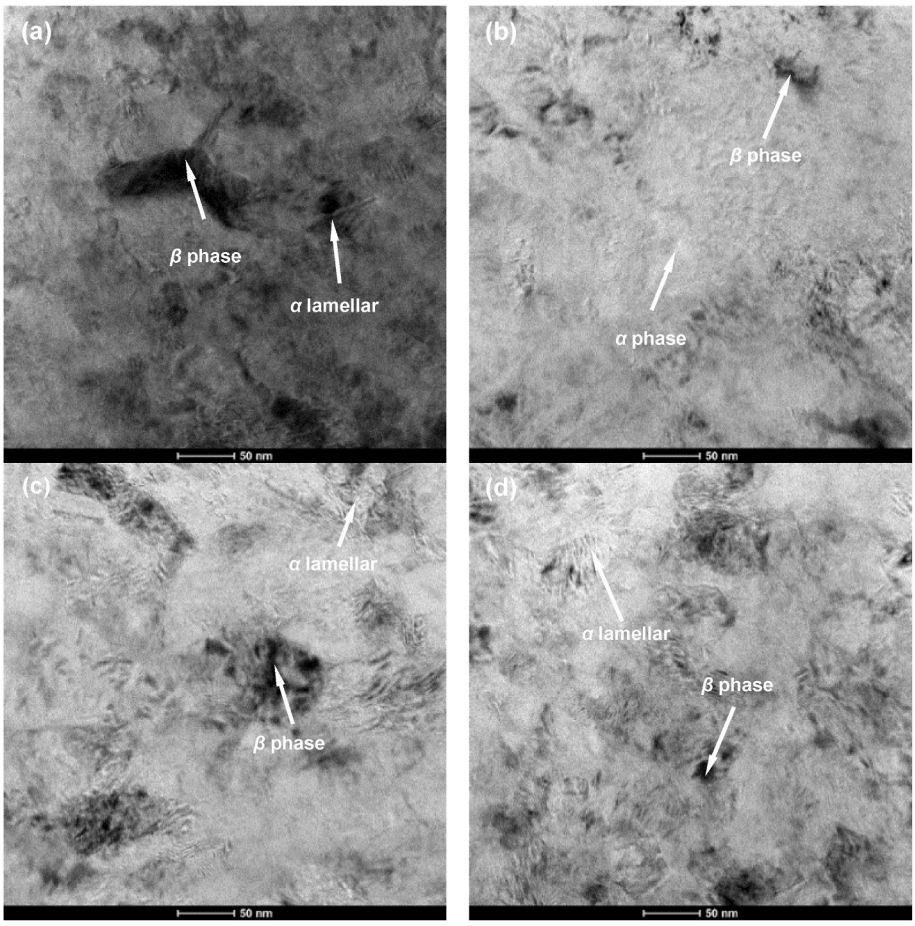

Fig. 10. Bright-field TEM images of the LSP-treated (a), UNSM-treated (b), LSP + UNSM-treated (c), and UNSM + LSP-treated (d) samples.

UNSM treatment is applied before LSP treatment, the initial plastic deformation and grain refinement from UNSM treatment are enhanced further by the CRS from LSP treatment. This sequence may induce even finer microstructural features than LSP + UNSM treatment, as UNSM treatment promotes a higher initial dislocation density and a finer microstructure before the LSP-induced CRS is applied. While SEM and EBSD are useful for larger-scale microstructural observations, TEM provides a deeper understanding at the nanoscale, revealing grain refinement and the distribution and morphology of the α and β phases.

3.7. Tribological performance

Fig. 11 shows the variation in COF of the untreated, LSP-treated, UNSM-treated, LSP + UNSM-treated and UNSM + LSP-treated samples as a function of sliding cycles. Running-in and steady-state friction characteristics were noticed for all the samples that interacted with a counterface ball. The untreated sample had a COF of 0.32 at the onset of the test that increased progressively over the 5000 sliding cycles. Later, it stabilized with a COF of 0.58 (see Fig. 11(a)) with considerable fluctuations throughout the test suggesting unstable frictional behavior. This increase in COF could indicate wear accumulation or surface degradation, leading to a rougher surface and higher resistance over time. The LSP-treated sample with a COF of 0.34 at the onset of the test demonstrated an increase during running-in and progressively increased with reciprocating cycles during running-in. Later, it also stabilized with a COF of 0.57 (see Fig. 11(b)). Fig. 11(c) shows the frictional behavior of the UNSM-treated sample. It was similar to the untreated and LSP-treated samples, the fluctuations were more controlled and less pronounced than in the untreated and LSP-treated samples. This indicates improved frictional stability and wear resistance, which may be mainly attributed to the reduced surface roughness showing that UNSM treatment helps maintain a lower and more stable COF over time. However, there is still a gradual increase, possibly due to surface changes with wear. Fig. 11(d and e) depict the COF of the LSP + UNSM-treated and UNSM + LSP-treated samples. The latter had a consistent COF with other samples, while the first decreased COF during both running-in and steady-state. Although there are fluctuations, they are less intense, and the overall COF remains relatively consistent over time, especially compared to untreated and LSP-treated samples. The UNSM + LSP treatment sequence showed relatively lower fluctuations than the LSP + UNSM treatment sequence. The combination of LSP and UNSM technologies likely reduced COF, resulting in a more stable frictional response than the untreated and LSP-treated samples. However, the UNSM-treated sample performed the best, maintaining a low and highly stable COF, indicating that the UNSM treatment may be optimal for wear resistance and frictional stability. The beneficial effect of UNSM treatment on the frictional behavior of SLM 316L has been previously noticed with a low COF due to the reduced surface roughness [22].

The inset of each Fig. 11(a–e) shows the SEM images of the samples and the counterface balls. As shown in Fig. 11(a), the wear track of the untreated sample shows significant roughness and wear debris, with evident grooves along the reciprocating sliding direction. These grooves indicate abrasive wear, where hard particles or asperities scrape against the surface, removing material from the surface. The wear mechanism of the untreated sample was also adhesion wear mode due to the difference in hardness of the sample and the counterface ball. The wear scar on the ball also shows severe wear with visible pits and grooves. The contact between the ball and the untreated sample likely led to material transfer and wear particle embedding. Predominantly abrasive wear, with potential for adhesive wear due to metal-to-metal contact, causing higher

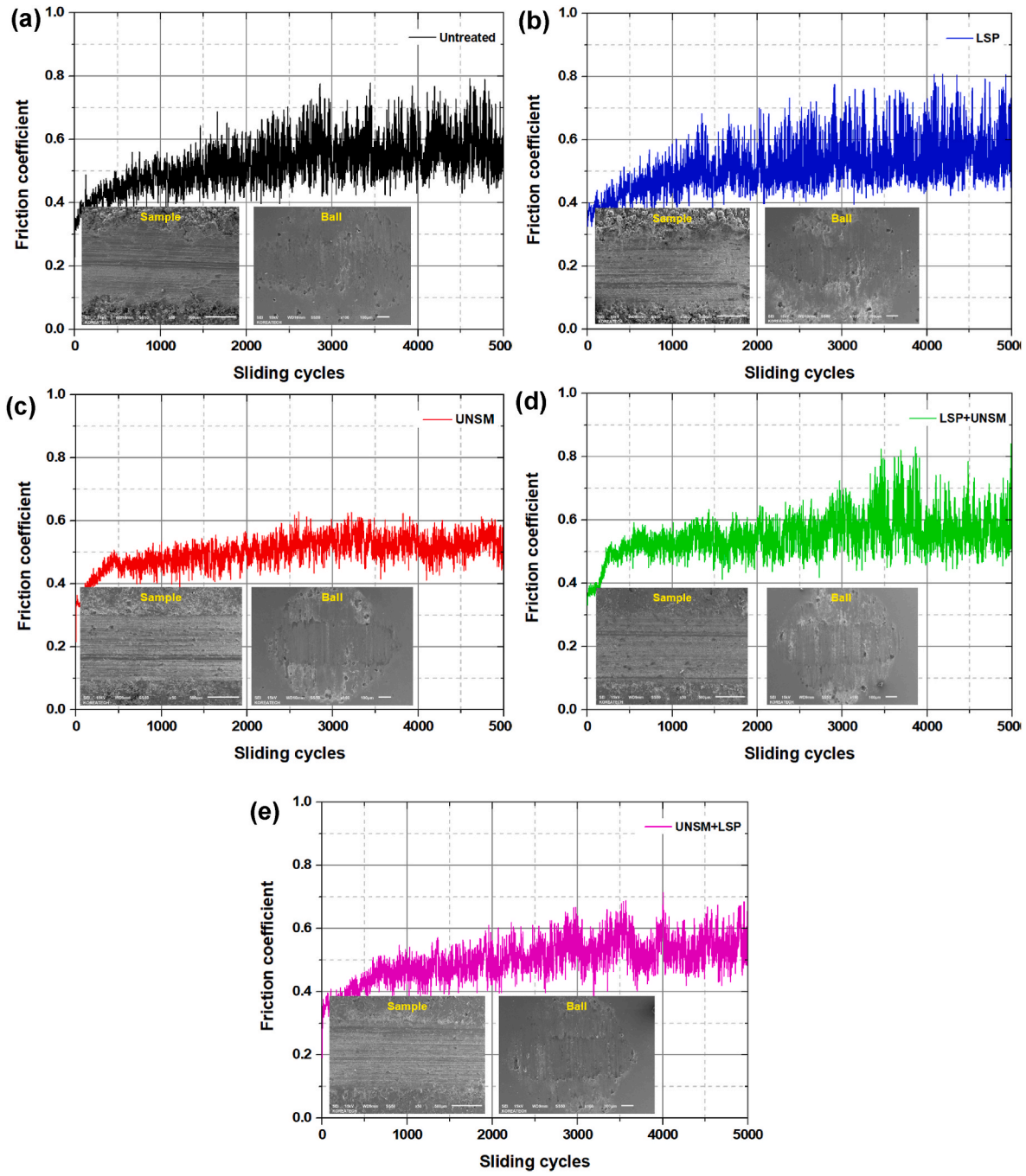

Fig. 11. COF of the untreated (a), LSP-treated (b), UNSM-treated (c), LSP + UNSM-treated (d), and UNSM + LSP-treated (e) samples.

wear debris and surface roughness. The LSP-treated sample shows a reduction in wear track roughness compared to the untreated sample, but grooves seem similar (see Fig. 11(b)). The wear scar of the counterface ball also appears somewhat a bit smoother than in the untreated case, with fewer pits and less intense wear features. While the abrasive wear mechanism was predominant, the LSP treatment appears to have strengthened the surface, reducing the extent of abrasive wear. Fig. 11 (c) shows the wear track of the UNSM-treated sample, which is smoother with much finer grooves, indicating improved surface hardness. The combination of two different abrasive and adhesive wear modes of the UNSM-treated sample was discovered, and the wear track depth was shallower than the untreated sample. The wear track shows relatively less wear debris and fewer signs of severe abrasion. The wear scar of the counterface ball was worn out in the central part, but some wear debris was attached to the center of the counterface ball. The wear scar of the counterface ball exhibits less material transfer and fewer pits compared to the untreated and LSP-treated samples. It is confirmed that UNSM treatment enhances surface hardness, leading to reduced abrasive wear. The smoother surface minimizes the interaction between asperities, decreasing both abrasive and adhesive wear mechanisms. Fig. 11(d) shows the wear track of the LSP + UNSM-treated sample. The wear track was even smoother than the previous cases, with fewer grooves and minimal wear debris. The combination of LSP and UNSM treatments enhanced the wear resistance compared to the untreated and LSP-treated samples, but not the UNSM-treated sample. The ball wear scar shows moderate damage, with a greater amount of material transfer or adhesion. The UNSM + LSP-treated sample showed the smoothest wear track among all the treatments as shown in Fig. 11(e). The ball wear area

in this treatment is the least affected, showing only mild wear marks and minimal material transfer, indicating effective wear resistance in the treated sample. This sequence of treatments (UNSM followed by LSP) appears to offer the best protection, primarily reducing abrasive and adhesive wear. The high surface hardness and CRS significantly decrease material loss and wear damage. The abrasive wear mechanism was predominant for the LSP + UNSM-treated and UNSM + LSP-treated samples, where the wear track size was found to be smaller than that of the untreated and LSP-treated samples, but more significant than the UNSM-treated sample. Moreover, the wear scar derived on the counter surface ball was worn out in the central part, but some wear debris was attached to the out of the central part of the counter surface ball. The combination of LSP and UNSM treatments appears to reduce abrasive wear synergistically. LSP treatment likely improves surface strength, while UNSM treatment further enhances hardness and smoothness, leading to minimal wear and reduced adhesion between the sample and the ball. Furthermore, it can be hypothesized that oxidative wear also occurred for all the samples. It was reported earlier that the primary wear mechanism of Ti-based alloys is abrasive, followed by adhesion and oxidation transferred layer [49].

The wear rate of the samples was measured based on the 3D images of the wear track as shown in Fig. 12. High wear depth and wide track width of the untreated sample shown in Fig. 12(a) suggested severe surface degradation under sliding, indicative of poor wear resistance. The LSP-treated samples had a similar wear track width compared to the untreated sample, but the depth of the wear track was shallower (see Fig. 12(b)). A considerable distinction in wear resistance was found as shown in Fig. 12(c), where the depth of the wear track of the UNSM-treated sample was shallower than other samples. The combination of LSP and UNSM technologies yields a balanced wear resistance (see Fig. 12(d)), likely benefiting from both CRS stress from LSP treatment and enhanced hardness from UNSM treatment. Although not as shallow as the UNSM-treated one, this combined treatment reduces both track width and depth, showing an improvement over the untreated and LSP-treated ones. Then, as shown in Fig. 12(e), the combined application of the UNSM + LSP technologies exhibited smaller wear track dimensions than those of the untreated, LSP-treated, and LSP + UNSM-treated samples. Still, it showed a deeper wear track than the UNSM-treated sample. The UNSM + LSP-treated sample provided better wear resistance than the LSP + UNSM-treated sample. The quantified wear rate of the samples is reported in Fig. 13. The wear rate of the untreated sample (3.57×10^{-8} $mm^3/N \times m$) was enhanced by approximately ~ 14.9% and 42.3% after LSP and UNSM technologies, respectively. The reduced wear depth and narrower track reflect improved wear resistance from UNSM treatment. Combined applications of UNSM + LSP and LSP + UNSM technologies could improve the wear resistance compared to the untreated and LSP-treated samples, but the UNSM-treated sample showed the best wear performance. It was found that the combined application of UNSM + LSP technologies showed better tribological performance than the combination of LSP + UNSM technologies, which is in connection with the change of crucial surface properties such as roughness and hardness after UNSM treatment.

4. Conclusions

Individual and combined applications of LSP and UNSM technologies

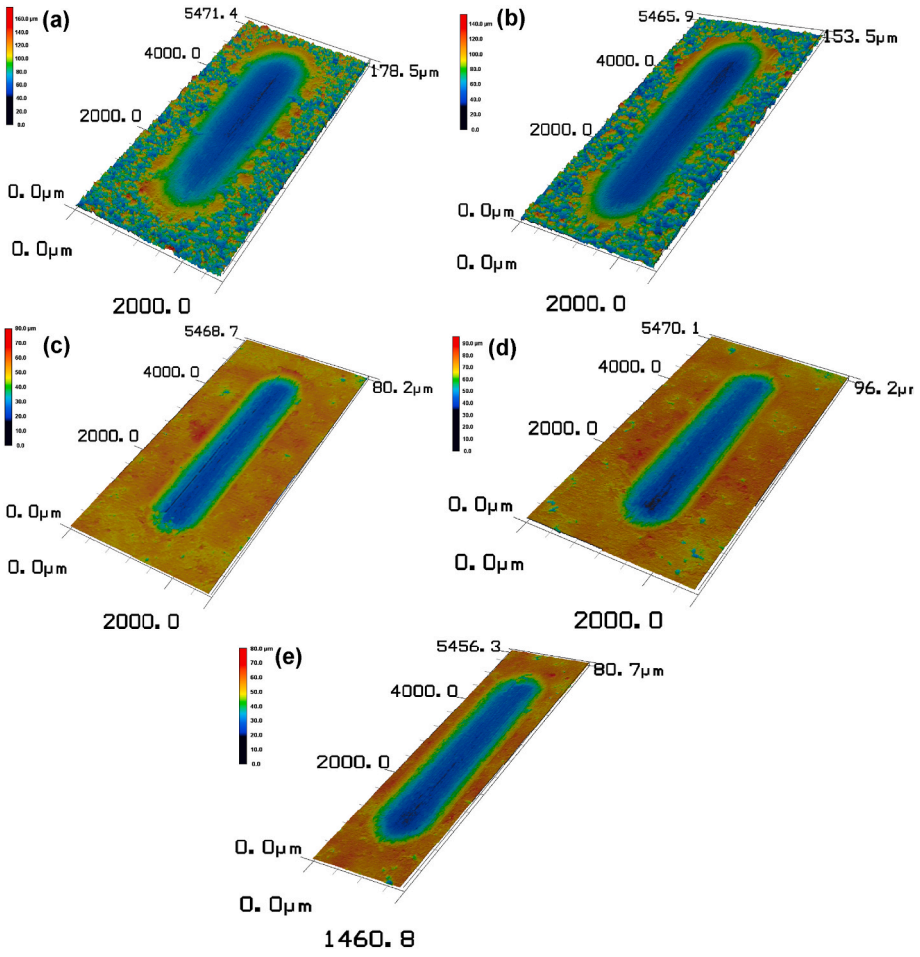

Fig. 12. 3D LSM images of the wear track formed on the surface of the untreated (a), LSP-treated (b), UNSM-treated (c), LSP + UNSM-treated (d), and UNSM + LSP-treated (e) samples.

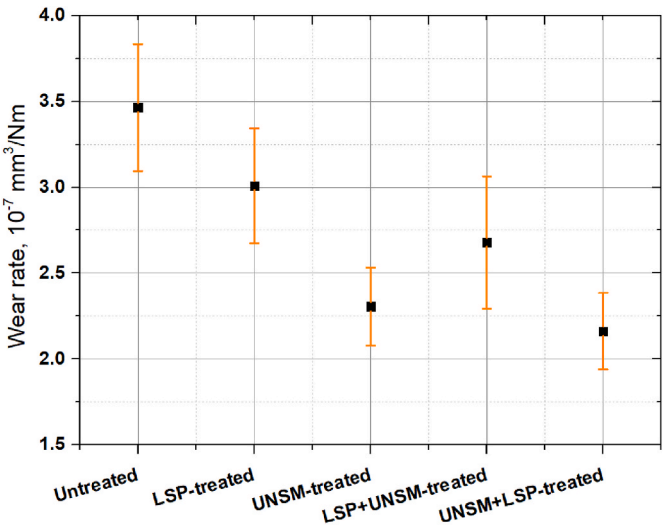

Fig. 13. Wear rate of the untreated, LSP-treated, UNSM-treated, LSP + UNSM-treated, and UNSM + LSP-treated samples.

were applied to Ti–6Al–4V alloy manufactured via the SLM process. The untreated sample exhibited a high surface roughness value of 9.96 ± 0.90 μm, which was increased to 12.10 ± 1.04 μm after LSP treatment, but it was reduced significantly to 1.07 ± 0.06 μm following UNSM treatment. When both LSP and UNSM technologies were applied in combination (LSP + UNSM and UNSM + LSP), the surface roughness was further reduced to 1.53 ± 0.25 μm and 1.60 ± 0.11 μm, respectively, but still higher than that of the UNSM-treated sample. The surface hardness of the LSP-treated and UNSM-treated samples was 343.3 HV and 352.0 HV, respectively. The average surface hardness, 364.4 HV, was observed in the LSP + UNSM-treated sample, while the UNSM + LSP-treated sample exhibited a slightly higher hardness of 367.3 HV. After both LSP and UNSM treatments, the surface TRS was converted to CRS. The LSP + UNSM-treated sample showed the highest CRS value of −705 MPa, similar to that of the UNSM-treated sample. Notably, the CRS introduced by UNSM treatment was partially mitigated by the subsequent LSP treatment. The wear rate of the LSP-treated and UNSM-treated samples decreased from 3.57×10^{-8} to 3.04×10^{-8} mm^3/N × m and 2.06×10^{-8} mm^3/N × m, respectively. The combined LSP + UNSM and UNSM + LSP treatments effectively reduced the COF and improved the wear resistance compared to untreated and LSP-treated samples. In conclusion, this paper introduces a novel approach combining two laser- and ultrasonic-based surface modification techniques - LSP and UNSM. The synergistic effects of these treatments in different order on microstructural changes, mechanical properties (including residual stress), and tribological performance have not been previously investigated. The originality of this work lies in demonstrating that the combination of LSP and UNSM technologies is more effective than their individual applications. This combined approach offers valuable insights into optimizing surface integrity and enhancing the durability of Ti–6Al–4V components produced by SLM as each method contributes uniquely to the surface and subsurface characteristics. The combination of the LSP and UNSM technologies is particularly beneficial for the fatigue performance and wear resistance of AMed parts, which often require improved surface quality and durability for demanding applications. The findings of this study are particularly relevant to researchers and practitioners in the field of AM and surface engineering, particularly those working with laser- and ultrasonic-based technologies for aerospace and nuclear applications.

Data availability

The data required to reproduce the results presented herein are available upon request.

Declaration of competing interest

The authors declare that they have no known competing financial interests or personal relationships that could have appeared to influence the work reported in this paper.

Acknowledgment

Open Access funding was supported by Tampere University and Tampere University Library.

References

[1] Kumar SA, Sundar R, Raman SGS, Kumar H, Gnanamoorthy R, Kaul R, Ranganathan K, Oak SM, Kukreja LM. Fretting wear behavior of laser peened Ti-6Al-4V. Tribol Trans 2012;55:615–23. https://doi.org/10.1080/10402004.2012.686087.
[2] Gorsse S, Hutchinson C, Gouné M, Banerjee R. Additive manufacturing of metals: a brief review of the characteristic microstructures and properties of steels, Ti-6Al-4V and high-entropy alloys. Sci Technol Adv Mater 2017;18:584–610. https://doi.org/10.1080/14686996.2017.1361305.
[3] Gu D, Hagedorn Y-C, Meiners W, Meng G, Batista RJS, Wissenbach K, Poprawe R. Densification behavior, microstructure evolution, and wear performance of selective laser melting processed commercially pure titanium. Acta Mater 2012;60:3849–60. https://doi.org/10.1016/j.actamat.2012.04.006.
[4] Thijs L, Verhaeghe F, Craeghs T, Humbeeck JV, Kruth J-P. A study of the microstructural evolution during selective laser melting of Ti–6Al–4V. Acta Mater 2010;58:3303–12. https://doi.org/10.1016/j.actamat.2010.02.004.
[5] Abe F, Osakada K, Shiomi M, Uematsu K, Matsumoto M. The manufacturing of hard tools from metallic powders by selective laser melting. J Mater Process Technol 2001;111:210–3. https://doi.org/10.1016/S0924-0136(01)00522-2.
[6] Mumtaz KA, Erasenthiran P, Hopkinson N. High density selective laser melting of Waspaloy®. J Mater Process Technol 2008;195:77–87. https://doi.org/10.1016/j.jmatprotec.2007.04.117.
[7] Ma C, Andani MT, Qin H, Moghaddam NS, Ibrahim H, Jahadakbar A, Amerinatanzi A, Ren Z, Zhang H, Doll GL, Dong Y, Elahinia M, Ye C. Improving surface finish and wear resistance of additive manufactured nickel-titanium by ultrasonic nano-crystal surface modification. J Mater Process Technol 2017;249:433–40. https://doi.org/10.1016/j.jmatprotec.2017.06.038.
[8] Shiomi M, Osakada K, Nakamura K, Yamashita T, Abe F. Residual stress within metallic model made by selective laser melting process. CIRP Annals 2004;53:195–8. https://doi.org/10.1016/S0007-8506(07)60677-5.
[9] Qiu C, Adkins NJE, Attallah MM. Microstructure and tensile properties of selectively laser-melted and of HIPed laser-melted Ti–6Al–4V. Mater Sci Eng 2013;578:230–9. https://doi.org/10.1016/j.msea.2013.04.099.
[10] Vilaro T, Colin C, Bartout JD, Nazé L, Sennour M. Microstructural and mechanical approaches of the selective laser melting process applied to a nickel-base superalloy. Mater Sci Eng 2012;534:446–51. https://doi.org/10.1016/j.msea.2011.11.092.
[11] Osakada K, Shiomi M. Flexible manufacturing of metallic products by selective laser melting of powder. Int J Mach Tool Manufact 2006;46:1188–93. https://doi.org/10.1016/j.ijmachtools.2006.01.024.
[12] Lee K-A, Kim Y-K, Yu J-H, Park S-H, Kim M-C. Effect of heat treatment on microstructure and impact toughness of Ti-6Al-4V manufactured by selective laser melting process. Arch Metall Mater 2017;62:1341–6. https://doi.org/10.1515/amm-2017-0205.
[13] Vilaro T, Colin C, Bartout JD. As-fabricated and heat-treated microstructures of the Ti-6Al-4V alloy processed by selective laser melting. Metall Mater Trans 2011;42:3190–9. https://doi.org/10.1007/s11661-011-0731-y.
[14] Ter Haar GM, Becker T, Blaine DC. Influence of heat treatments on the microstructure and tensile behaviour of selective laser melting-produced Ti-6Al-4V parts. S Afr J Ind Eng 2016;27. https://doi.org/10.7166/27-3-1663.
[15] Vrancken B, Thijs L, Kruth J-P, Van Humbeeck J. Heat treatment of Ti6Al4V produced by selective laser melting: microstructure and mechanical properties. J Alloys Compd 2012;541:177–85. https://doi.org/10.1016/j.jallcom.2012.07.022.
[16] Bhaduri D, Penchev P, Batal A, Dimov S, Soo SL, Sten S, Harrysson U, Zhang Z, Dong H. Laser polishing of 3D printed mesoscale components. Appl Surf Sci 2017;405:29–46. https://doi.org/10.1016/j.apsusc.2017.01.211.
[17] Rosa B, Mognol P, Hascoët J. Laser polishing of additive laser manufacturing surfaces. J Laser Appl 2015;27:S29102. https://doi.org/10.2351/1.4906385.
[18] Aguado-Montero S, Navarro C, Vazquez J, Lasagni F, Slawik S, Dominquez J. Fatigue behavior of PBF additive manufactured Ti6Al4V alloy after shot and laser peening, vol. 154; 2022, 106536. https://doi.org/10.1016/j.ijfatigue.2021.106536.
[19] Ma CP, Guan YC, Zhou W. Laser polishing of additive manufactured Ti alloys. Opt Laser Eng 2017;93:171–7. https://doi.org/10.1016/j.optlaseng.2017.02.005.
[20] Maleki E, Unal O, Guagliano M, Bagherifad S. The effects of shot peening, laser shock peening and ultrasonic nanocrystal surface modification on the fatigue

strength of Inconel 718. Mater Sci Eng 2021;810:141029. https://doi.org/10.1016/j.msea.2021.141029.
[21] Amanov A, Cho I-S, Kim D-E, Pyun Y-S. Fretting wear and friction reduction of CP titanium and Ti–6Al–4V alloy by ultrasonic nanocrystalline surface modification. Surf Coating Technol 2012;207:135–42. https://doi.org/10.1016/j.surfcoat.2012.06.046.
[22] Amanov A. Effect of local treatment temperature of ultrasonic nanocrystalline surface modification on tribological behavior and corrosion resistance of stainless steel 316L produced by selective laser melting. Surf Coating Technol 2020;398:126080. https://doi.org/10.1016/j.surfcoat.2020.126080.
[23] Amanov A, Urmanov B, Amanov T, Pyun YS. Strengthening of Ti-6Al-4V alloy by high temperature ultrasonic nanocrystal surface modification technique. Mater Lett 2017;196:198–201. https://doi.org/10.1016/j.matlet.2017.03.059.
[24] [a] Lim H, Kim P, Jeong H, Jeong S. Enhancement of abrasion and corrosion resistance of duplex stainless steel by laser shock peening. J Mater Process Technol 2012;212:1347–54. https://doi.org/10.1016/j.jmatprotec.2012.01.023.[b] Sano Y, Obata M, Kubo T, Mukai N, Yoda M, Masaki K, Ochi Y. Retardation of crack initiation and growth in austenitic stainless steels by laser peening without protective coating. Mater Sci Eng 2006;417:334–40. https://doi.org/10.1016/j.msea.2005.11.017.
[25] Sano Y. Laser peening without coating as a surface enhancement technology. Journal of Laser Micro/Nanoengineering. 2006;1:161–6. https://doi.org/10.2961/jlmn.2006.03.0002.
[26] Zhang H, Dong D, Su S, Chen A. Experimental study of effect of post processing on fracture toughness and fatigue crack growth performance of selective laser melting Ti-6Al-4V. Chin J Aeronaut 2019. https://doi.org/10.1016/j.cja.2018.12.007.
[27] Maleki E, Bagherifard S, Unal O, Jam A, Shao S, Guagliano M, Shamsaei N. Superior effects of hybrid laser shock peening and ultrasonic nanocrystalline surface modification on fatigue behavior of additive manufactured AlSi10Mg. Surf Coating Technol 2023;463:129512. https://doi.org/10.1016/j.surfcoat.2023.129512.
[28] Qiao H, Zhao J, Gao Y. Experimental investigation of laser peening on TiAl alloy microstructure and properties. Chin J Aeronaut 2015;28:609–16. https://doi.org/10.1016/j.cja.2015.01.006.
[29] Wang Z, Yang S, Peng Z, Gao Z. Effect of defects in laser selective melting of Ti-6Al-4V alloy on microstructure and mechanical properties after heat treatment. Opt Laser Technol 2022;156:108522. https://doi.org/10.1016/j.optlastec.2022.108522.
[30] Dai F, Zhou J, Lu J, Luo X. A technique to decrease surface roughness in overlapping laser shock peening. Appl Surf Sci 2016;370:501–7. https://doi.org/10.1016/j.apsusc.2016.02.138.
[31] Bagehorn S, Wehr J, Maier HJ. Application of mechanical surface finishing processes for roughness reduction and fatigue improvement of additively manufactured Ti-6Al-4V parts. Int J Fatig 2017;102:135–42. https://doi.org/10.1016/j.ijfatigue.2017.05.008.
[32] Navarro Pintado Carlos, Vázquez Jesús, Domínguez Jaime, Periñán Antonio, Herrera García Marta, Lasagni Fernando, Bernarding Simon, Slawik Sebastian, Mücklich Frank, Boby Francisco, Hackel Lloyd. Effect of surface treatment on the fatigue strength of additive manufactured Ti6Al4V alloy. Frat Ed Integrità Strutt 2020;14:337–44. https://doi.org/10.3221/IGF-ESIS.53.26.
[33] Zhang XC, Zhang YK, Lu JZ, Xuan FZ, Wang ZD, Tu ST. Improvement of fatigue life of Ti–6Al–4V alloy by laser shock peening. Mater Sci Eng 2010;527:3411–5. https://doi.org/10.1016/j.msea.2010.01.076.
[34] Zhang H, Chiang R, Qin H, Ren Z, Hou X, Lin D, Doll GL, Vasudevan VK, Dong Y, Ye C. The effects of ultrasonic nanocrystal surface modification on the fatigue performance of 3D-printed Ti64. Int J Fatig 2017;103:136–46. https://doi.org/10.1016/j.ijfatigue.2017.05.019.
[35] Żebrowski R, Walczak M, Korga A, Iwan M, Szala M. Effect of shot peening on the mechanical properties and cytotoxicity behaviour of titanium implants produced by 3D printing technology. Journal of Healthcare Engineering 2019;2019:1–11. https://doi.org/10.1155/2019/8169538.
[36] Żebrowski R, Walczak M. Effect of the shot peening on surface properties and tribological performance of Ti-6Al-4V alloy produced by means of DMLS technology. https://doi.org/10.24425/AMM.2019.126263; 2019.
[37] Amanov A, Karimbaev R, Maleki E, Unal O, Pyun Y-S, Amanov T. Effect of combined shot peening and ultrasonic nanocrystal surface modification processes on the fatigue performance of AISI 304. Surf Coating Technol 2019;358:695–705. https://doi.org/10.1016/j.surfcoat.2018.11.100.
[38] Ahn D-H, Kim W, Kang M, Park LJ, Lee S, Kim HS. Plastic deformation and microstructural evolution during the shock consolidation of ultrafine copper powders. Mater Sci Eng 2015;625:230–44. https://doi.org/10.1016/j.msea.2014.12.012.
[39] Li Y, Sun K, Liu P, Liu Y, Chui P. Surface nanocrystallization induced by fast multiple rotation rolling on Ti-6Al-4V and its effect on microstructure and properties. Vacuum 2014;101:102–6. https://doi.org/10.1016/j.vacuum.2013.07.028.
[40] Zhou W, Ren X, Liu F, Ren Y, Li L. Nanocrystallization in the duplex Ti-6Al-4V alloy processed by multiple laser shock peening. Metals 2016;6:297. https://doi.org/10.3390/met6120297.
[41] Tan X, Kok Y, Toh WQ, Tan YJ, Descoins M, Mangelinck D, Tor SB, Leong KF, Chua CK. Revealing martensitic transformation and α/β interface evolution in electron beam melting three-dimensional-printed Ti-6Al-4V. Sci Rep 2016;6. https://doi.org/10.1038/srep26039.
[42] Liu Y, Yang Y, Wang D. A study on the residual stress during selective laser melting (SLM) of metallic powder. Int J Adv Des Manuf Technol 2016;87:647–56. https://doi.org/10.1007/s00170-016-8466-y.
[43] Gao YK. Improvement of fatigue property in 7050–T7451 aluminum alloy by laser peening and shot peening. Mater Sci Eng 2011;528:3823–8. https://doi.org/10.1016/j.msea.2011.01.077.
[44] Ren XD, Zhang YK, Yongzhuo HF, Ruan L, Jiang DW, Zhang T, Chen KM. Effect of laser shock processing on the fatigue crack initiation and propagation of 7050-T7451 aluminum alloy. Mater Sci Eng 2011;528:2899–903. https://doi.org/10.1016/j.msea.2010.12.058.
[45] Karimbaev R, Pyun YS, Amanov A. Fatigue life extension of additively manufactured Nickel-base 718 alloy by nanostructured surface. Mater Sci Eng 2022;831:142041. https://doi.org/10.1016/j.msea.2021.142041.
[46] Lu K. Making strong nanomaterials ductile with gradients. Science 2014;345:1455–6. https://doi.org/10.1126/science.1255940.
[47] Ye C, Telang A, Gill AS, Suslov S, Idell Y, Zweiacker K, Wiezorek JMK, Zhou Z, Qian D, Mannava SR, Vasudevan VK. Gradient nanostructure and residual stresses induced by ultrasonic nano-crystal surface modification in 304 austenitic stainless steel for high strength and high ductility. Mater Sci Eng 2014;613:274–88. https://doi.org/10.1016/j.msea.2014.06.114.
[48] Jones MR, Nation BL, Wellington-Johnson JA, Curry JF, Kustas AB, Lu P, Chandross M, Argibay N. Evidence of inverse Hall-Petch behavior and low friction and wear in high entropy alloys. Sci Rep 2020;10. https://doi.org/10.1038/s41598-020-66701-7.
[49] Molinari A, Straffelini G, Tesi B, Bacci T. Dry sliding wear mechanisms of the Ti6Al4V alloy. Wear 1997;208:105–12. https://doi.org/10.1016/S0043-1648(96)07454-6.